Robust Decadal Variations in ENSO Diversity, and its Impact on Future Scenarios

Bastien Dieppois[1, 2]*, Antonietta Capotondi[3, 4], Benjamin Pohl [5], Kwok Pan Chun[6], Paul-Arthur Monerie[7], Jonathan Eden[1]

[1] Centre for Agroecology, Water and Resilience, Coventry University, Coventry, UK

[2] Department of Oceanography, MARE Institute, University of Cape Town, Cape Town, RSA

[3] Cooperative Institute for Research in Environmental Sciences, University of Colorado, Boulder, Colorado, USA

[4] Physical Sciences Laboratory, NOAA, Boulder, Colorado, USA

[5] Centre de Recherches de Climatologie, UMR 6282 Biogéosciences, CNRS/Université de Bourgogne Franche Comté, Dijon, France

[6] Department of Geography, Hong Kong Baptist University, Hong Kong, China

[7] Department of Meteorology, National Centre for Atmospheric Science (NCAS), University of Reading, Reading, UK

*Correspondence to: Bastien Dieppois, Centre for Agroecology, Water and Resilience (CAWR), Coventry University, Ryton Gardens, Ryton on Dunsmore, Coventry, CV8 3LG, UK. E-mail: bastien.dieppois@coventry.ac.uk

Abstract

El Niño-Southern Oscillation (ENSO) shows a large diversity of events, whose modulation by climate variability and change, and their representation in climate models, limit our ability to predict their impact on ecosystems and human livelihood. Here, we introduce a new framework to analyze probabilistic changes in event-location and -intensity, which overcomes existing limitations in studying ENSO diversity. We find robust decadal variations in event intensities and locations in century-long observational datasets, which are associated with perturbations in equatorial wind-stress and thermocline depth, as well as extra-tropical anomalies in the North and South Pacific. A large fraction of CMIP5 and CMIP6 models appear capable of simulating such decadal variability in ENSO diversity, and the associated large-scale patterns. Projections of ENSO diversity in future climate change scenarios strongly depend on the magnitude of decadal variations, and the ability of climate models to reproduce them realistically over the 21st century.

Introduction

El Niño-Southern Oscillation (ENSO) is the leading mode of tropical climate variability, with impacts on ecosystems, agriculture, freshwater supplies and hydropower production spanning much of the globe[1–3]. The majority of impact studies, including seasonal to multi-year predictions, have developed from a "canonical" representation of ENSO, as characterised by sea-surface temperature anomalies (SSTa) in the central-eastern Pacific[4–6]. However, ENSO shows large differences from one event to another in terms of its intensity, spatial patterns and temporal evolutions[7–9]. For instance, while the 1997/98 El Niño displayed extreme SSTa in the eastern equatorial Pacific (EP-ENSO), the largest SSTa in the winter of 2002/03 were weaker and primarily confined to the central equatorial Pacific (CP-ENSO). Differences in the longitudinal location and intensity of ENSO events are sensitively associated with different

impacts on regional climate throughout the world[10,11]. Such differences in ENSO patterns, referred to as "ENSO diversity"[7], and their representation in climate models thus strongly influence the skill of impact prediction systems[12], and underscore the need for an appropriate characterization and further mechanistic understanding of ENSO diversity.

The post-1990s increases in the frequency of CP El-Niño events[13–15] has led some researchers to associate such changes in ENSO patterns to the influence of global warming[16]. However, the role of natural low-frequency climate variations may also be important for altering ENSO characteristics[17–19]. Indeed, observations and climate models show the presence of decadal modulations in both intensity[17,19,20] and pattern diversity[21]. In particular, different phases of the Pacific Decadal Oscillation (PDO)[18,22] and the Atlantic Multidecadal Oscillation (AMO)[23] were considered more conducive to either CP- or EP-ENSO. However, to date, no robust decadal variation in event locations has been detected in long-term observational records[24,25]. Similarly, we know very little about the ability of climate models to realistically reproduce ENSO diversity and its low-frequency variability[7,8]. CMIP3 and CMIP5 models showed large biases in the background mean state of equatorial Pacific SST, leading to an excessive westward extension of the ENSO patterns[26–28], and limiting the models' ability to simulate realistic ranges of ENSO diversity[9,29]. Further research is thus needed to determine how these decadal variations may affect the reported historical and future strengthening of ENSO[30–32], as well as the increasing occurrence of CP- versus EP-events[13–16].

Studying ENSO diversity has however been largely limited by various technical shortcomings. Such studies are traditionally based on several indices of tropical Pacific SSTa, designed to monitor the variability of either a "canonical" ENSO or two extreme ENSO flavours[33–37]. Yet, these indices emphasize El Niño events, while La Niña events, which are associated with

weaker anomalies than El Niño events[38], are typically located further West[7] and tend to show a more limited range of pattern diversity[39], have received less attention. Hence, traditional indices tend to neglect the existing asymmetry between warm- and cold-phases, and between CP- and EP-events. Besides, most of these indices are significantly inter-correlated (Fig.1a), suggesting that they provide redundant information on ENSO. More importantly, the probability distribution of the peak location of SSTa over the tropical Pacific (when each index is exceeding ±0.5°C standard deviation; Fig.1b), indicates that most of these indices are neither representing solely CP- and EP-events, but rather different combinations of both ENSO flavours.

#Figure 1#

It is therefore essential to develop a new framework allowing for a more precise assessment of changes in the location and intensity of warm- and cold ENSO events. In this regard, the "Center of Heat Index" (CHI) provided the basis for a more flexible framework, allowing the longitudinal centre of SSTa to vary as a function of time instead of being geographically fixed[24,25]. Yet, the CHI approach defines El Niño (La Niña) events based on anomalously warm (cold) areas over very large longitudinal extents (> ~5550km), hereby yielding a very smooth representation of ENSO diversity, and limiting the detectable ranges of spatial patterns. Here, we introduce a novel "non-parametric" framework to allow for a more precise assessment of probabilistic changes in ENSO diversity, notably in event locations and intensity (cf. Methods). This new framework is first applied to a suite of observational datasets, including century-long reconstructions, reanalysis and high-resolution satellite-derived estimates (cf. Supplementary Table 1), to identify potential long-term changes in the likelihood of El Niño and La Niña location and intensity, and discuss their associations with decadal climate variability. The same framework is then applied to the two latest multi-model ensembles, *i.e.* CMIP5[40] and CMIP6[41] (cf. Supplementary Table 1), to examine how model fidelity in simulating ENSO diversity is

influenced by using an approach that allows for a continuum of patterns, rather than relying on a more rigid bimodal view of the ENSO phenomenon. Historical and multi-centennial pre-industrial control simulations (piControl: 400–1200 years, radiative forcing fixed at the 1850 conditions) are used to examine whether robust decadal variations can be found in the absence of anthropogenic influences (piControl) or under historical radiative forcing (historical). The large-scale climate patterns associated with decadal variations in ENSO diversity are examined in both observations and in the climate models that most realistically simulate ENSO diversity and its low-frequency variability in pre-industrial and historical periods. The same models are then used to assess how ENSO diversity is projected to change in the future. In particular, we address two questions: i) do ENSO events really strengthen and shift westward in the 21st century? ii) if so, is that true for both El Niño and La Niña events?

Results

Observed changes in the likelihood of ENSO location and intensity

The average distribution of ENSO location and intensity in 20-year overlapping periods between 1850 and 2017, is examined using five observational datasets (Fig. 2).

#Figure 2#

On average, El Niño events tend to be located over three preferential regions (Fig. 2a): i) in the central Pacific (~166°W; CP-Niño); ii) in a region corresponding to a "canonical" pattern (~118°W; Canonical-Niño); iii) off the coast of southern America, in the eastern Pacific (~ 85°W; EP-Niño). EP-Niño, or coastal-Niño[42], are much less likely in all datasets, especially in the satellite-derived data (OISST.v2; Fig. 2a, top-left). Accounting for temporal changes in the probability distribution of all datasets, we identify a coherent and progressive shift to predominant CP-Niño event over the course of the 20th century (Fig. 2a, bottom-left). La Niña also appears characterized by three preferential locations, with no significant differences in the

probability distribution from one dataset to another (Fig. 2b, top-left). CP-Niña events seem systematically more likely than Canonical-Niñas, which are in turn more likely than EP-Niñas (Fig. 2b, top-left). Looking at temporal changes in the statistical distribution across all datasets, coherent low-frequency variations emerge in the most likely locations of La Niña (Fig. 2b, bottom-left). CP-Niña events are more frequent in the 1930s-40s and from the 1970s than during the 1950s-60s (Fig. 2b, bottom-left).

All observational datasets show quasi-normal distributions for event intensity, converging toward SSTa of +0.86°C and -0.9°C for El Niño and La Niña events, respectively (Fig. 2a-b, top-right). In all observational datasets, the probability distribution of La Niña intensity shows relatively small variations over time (Fig. 2b, bottom-right), while decadal variations prevail for El Niño intensity (Fig. 2a, bottom-right). Weaker El Niño are more likely in the late 19th century, the 1920s-50s and 1980s-90s, as compared to the early 20th century, the 1960s-70s and post-2000s (Fig. 2a, bottom-right). Both El Niño and La Niña events show increasing intensities over recent decades, and this is associated with more extreme events, as illustrated by the increasing frequency of extreme warm and cold events (Fig. 2a-b, histograms, bottom-left). This result is consistent with coral oxygen isotopic reconstructions[32] and simulated long-term future changes[30,31]. However, unlike the recent increase in the frequency of extreme La Niña, the intensification of El Niño events does not seem to exceed a natural range of variability (Fig. 2a-b, bottom-right). These results, based on multiple and longer observational records, partly corroborate those of a recent study, highlighting more extreme El Niño and La Niña in the 1980s-90s than in the post-2000 period using OISSTv.2[43].

Hence, observed ENSO diversity is much broader than previously suggested, and exceeds a bimodal view, consistently with results from neural-network based clustering of equatorial

Pacific SSTa[44]. This is particularly true for La Niñas, whose diversity was strongly questioned in previous studies[39]. More importantly, ENSO-event locations do not follow a normal distribution describing a randomly distributed continuum of events[24], converging toward a "canonical" location. Instead, ENSO diversity is clearly linked to low-frequency variations, with multiple preferential locations, which may modulate potential trends in ENSO behaviour.

Evaluation of ENSO diversity in climate models within our new framework

We compare the simulated probability distributions of ENSO location and intensity from 26 CMIP5 and 28 CMIP6 models to our five observational datasets in Fig. 3.

#Figure 3#

Most models are capable of simulating a broad range of preferred locations for both El Niño and La Niña (Fig. 3a-b, top), and around 39–60% of simulations do not show significant biases in the mean location of El Niño and La Niña in historical and piControl runs (Supplementary Fig. 1). In particular, two CMIP6 models (IPSL-CM6A-LR and UKESM1-0-LL, one of the MOHC group of models) show a range of locations for both warm- and cold-events that is in good agreement with observations (Fig. 3, top). Similar results are found for CNRM-CM5 (leftmost columns of the CNRM group of models), but only for El Niño events (Fig. 3, top). Other models show highly asymmetrical probability distributions, with clear tendencies to favour either EP/Canonical- or CP-events (Fig. 3a-b, top), including some extreme cases (e.g. CSIRO-Mk3-6-0) with events always centred further west than the observational range. The excessive westward extensions of the equatorial SSTa[26–28] could explain the westward shifted mean location of ENSO in CMIP models. Here only 16–30% of model simulations are concerned by this bias (Supplementary Fig. 1). Nevertheless, there are other models that do not simulate erroneous westward extensions of the equatorial SSTa, but hardly depart from a

canonical location (Fig. 3a-b, top; Supplementary Fig. 1), thus showing too limited ENSO diversity.

Simulated intensity distributions of ENSO are mostly consistent with observations, and tend to follow a quasi-normal distribution in most CMIP5 and CMIP6 models, but clear discrepancies emerge in the mean intensity and the probability of extreme events (Fig. 3a-b, bottom). In 53 –66% of the simulations, biases in the mean intensity of ENSO events are non-significant for warm- and cold-events, using both historical and piControl simulations (Supplementary Fig. 1). Large and significant overestimations and underestimations nevertheless persist in a little less than half of the models (Supplementary Fig. 1).

In summary, most models simulate some range of pattern diversity for El Niño and La Niña events. In particular, few models present a range of event locations in relatively good agreement with observations, and minimal biases in their intensity. The most common biases concern either the tendency of models to favour one type of events or the events' intensity. Notably, larger biases are found for the models that produce erroneous westward extensions of SSTa (cf. MIROC6, Supplementary Figs. 2-5).

Robust decadal variations in ENSO preferred location and intensity

Here, we use spectral analysis to examine whether robust and significant low-frequency variations are found in the most likely location and intensity of ENSO, in both the four long-term observational datasets, as well as CMIP5 and CMIP6 models. We first examine the timescales on which ENSO behaviour varies using maximum power spectrum (See methods, Fig. 4), a method that accounts for non-stationarity of ENSO spectral characteristics, before

comparing the observed and simulated magnitude of decadal variations in location and intensity (Fig. 5).

#Figure 4#

Despite some discrepancies, all observational datasets show significant variations on interdecadal timescale (14–32-yr) based on the 10-yr running mean of most likely location of El Niño and La Niña (Fig. 4a-b, top-right). Using both historical and piControl runs, almost all models also show significant variability on interdecadal timescales in their 10-yr most likely location of ENSO (Fig. 4a-b, top-middle and -left). In addition, 71 and 72 (83 and 87) % of historical (piControl) runs significantly simulate statistically equal decadal variance, as compared to observations, in the locations of El Niño and La Niña, respectively (Fig. 5). Few models show significant biases in the magnitude of decadal variations in event locations (Fig. 5): i) 9–25% of models underestimate it, and favour either EP/Canonical- (*e.g.*, CCCma models, CNRM-CM6-1) or CP-ENSO (*e.g.*, CESM2); or ii) 2–11% of models overestimate it, and tend to simulate two extremely distinct modes in the central and eastern Pacific (*e.g.*, MIROC6, NorCPM1; Fig. 3a-b, top).

#Figure 5#

According to previous observational studies[45], as well as fossil coral oxygen isotope records[32], the observed intensity of ENSO presents significant variability on interdecadal timescales at 16-yr and, especially, 32-yr periods (Fig. 5a-b, bottom-right). CMIP5 and CMIP6 also simulate significant interdecadal variability at these timescales (Fig. 5, bottom-middle and -left), in agreement with previous studies using climate models[17,20,21]. Most models (63–85% in historical and piControl runs) display statistically equal decadal variance in the intensity of both El Niño and La Niña (Fig. 5), in agreement with observations. A small fraction of simulations (12–24% in historical and piControl runs) significantly overestimate the decadal variance in ENSO intensity (Fig. 5), as already reported for CCSM4[46] and CESM2[47].

Thus, our results confirm the existence of a significant interdecadal modulation in ENSO intensity in accordance with several studies based on observations, proxy records and climate models[17,20,21,24,32,45]. While previous studies reported an underestimation of decadal variability by climate models at both global[48] and Pacific Ocean[49,50] scales, this statement does not appear to be true for ENSO diversity in most CMIP5 and CMIP6 models, when considering their non-stationary behaviour (cf. Methods). Our results also reveal, for the first time, significant interdecadal modulations in the maximum likelihood of ENSO locations, which are robust and consistent in both observations and climate models. In addition, although few models show recurrent biases, the majority of models appear capable of simulating realistic magnitudes of decadal variance in ENSO diversity.

Large-scale patterns linked decadal variability in ENSO location and intensity

To identify large-scale patterns of variability associated with spatio-temporal variations in ENSO, separately for El Niño years and La Niña years, we compute linear regressions of pan-Pacific SSTa, wind-stress and equatorial 20°C isotherm depth (Z20) on the location and intensity of events, using four long-term observational datasets and 32 historical runs from the IPSL-CM6A-LR large ensemble (Fig. 6). We focus on the Pacific region, as regressed SSTa are much lower, and often non-significant, in the other ocean basins (not shown). Similarly, we choose to focus on the IPSL-CM6A-LR model because it provides a realistic range of locations and intensities for both El Niño and La Niña events, with relatively weak model biases (Figs. 3-4). Results obtained using other CMIP5 and CMIP6 models are highly similar, especially for patterns associated with ENSO intensity, and approximate the skill of the SODA.si3 reanalysis (Supplementary Figs. 2-3).

#Figure 6#

In observations, SST regressions on El Niño longitude yield an EP-type event, with largest anomalies extending westward along the Equator from the coast of South America (Fig. 6a, top-left). The associated strong westerly wind anomalies extend to the eastern Pacific, where the thermocline is significantly deeper, whilst slight, but significant, easterly wind anomalies and shallower thermocline are found in the western Pacific (Fig. 6a, top- and bottom-left). These patterns indicate that El Niño events tend to be located further east when trade-winds weaken (strengthen), and the thermocline is significantly deeper (shallower), over the eastern (western) Pacific; meanwhile, the opposite patterns would be associated with El Niño events located further West. This is consistent with previous studies stressing the importance of the initial zonal thermocline slope as a discriminating factor for the selection of EP and CP events[51]. Compared to regression patterns associated with El Niño longitude, regressions on La Niña longitude show much stronger (weaker) signals in the western-central (eastern) Pacific (Fig. 6a-b, top-left). However, such differences could originate from differences in the probability distributions of El Niño and La Niña locations (Fig. 2a-b, top-left). Regressions on La Niña longitude result in a pattern that is reminiscent of a CP-Niño pattern[37], with cold anomalies in the far eastern Pacific and warm anomalies in the central Pacific (Fig. 6b, top-left). In this case, strong westerly wind anomalies and deeper thermocline are found in the central Pacific, where they may contribute to the zonal advective feedback[52], while weaker easterly anomalies and deeper thermocline are present in the western Pacific (Fig. 6b, top- and bottom-left). Such patterns indicate that La Niña events tend to be located further east when trade-winds strengthen (weaken), and the thermocline is significantly shallower (deeper), over the eastern (western) Pacific; the opposite patterns would thus favour more western La Niña events. In addition, these tropical signals are statistically significantly related to extra-tropical SSTa (Fig. 6a-b): colder (warmer) North Pacific SSTa are found, when El Niño events are located further east (west), and La Niña events are located further west (east). While these

results corroborate previous study on changes in the frequency of CP and EP events during different phases of the PDO[22,53], such North Pacific SSTa are also consistent with changes in the intensity and location of the Aleutian Low and North Pacific High in response to EP- and CP-Niño[54]. Similar regression patterns are found in IPSL-CM6A-LR, and other models (Supplementary Figs. 2-3), which can produce realistic changes in zonal wind-stress and thermocline depth, associated with shifts in ENSO locations (Fig. 6c). Patterns associated with changes in El Niño and El Niña locations are however much more symmetrical in models than in observation (Fig. 6c; Supplementary Figs. 2-3). Like other models, IPSL-CM6A-LR shows large internal variability in thermocline depth anomalies, with a clear tendency to underestimate thermocline depth anomalies during El Niño events (Supplementary Fig. 4), and this could explain larger ensemble spread in equatorial Pacific SSTa associated with shifting ENSO locations (Fig. 6c). The North Pacific anomalies associated with ENSO locations are also significant in IPSL-CM6A-LR (Fig. 6c), like in many other models (Supplementary Fig. 3). These relationships between ENSO and Pacific extra-tropical variability however show large ensemble spread in IPSL-CM6A-LR (Fig. 6c), highlighting that these relationships are highly sensitive to internal variability, as suggested in previous studies[22,55].

Looking at regressed patterns associated with event intensity, patterns of SST anomalies are more in line with canonical events, extending in the central-eastern Pacific, for both El Niño and La Niña (Fig. 6a-b, top-right). In addition, we found that observed El Niño (La Niña) is more intense when the mean thermocline is deeper (shallower) and the trade-winds are consistently weaker (stronger) over the equatorial Pacific (Fig. 6a-b, top- and bottom-right). Compared to the large-scale patterns associated with ENSO locations, changes in ENSO intensity are associated with larger wind-stress and thermocline depth anomalies over the central-eastern equatorial Pacific (Fig. 6a-b). ENSO intensity also appears associated with

extra-tropical SST and wind anomalies that are more symmetric about the Equator compared to those associated with the location (Fig. 6a-b), and are somewhat reminiscent of the extra-tropical signature of the Interdecadal Pacific Oscillation[56] (IPO). Other studies discussed the separate importance of North and South Pacific climate variability on ENSO intensity at interannual to decadal timescales[55,57]. Although it systematically underestimates both zonal wind-stress and Z20 anomalies compared to observations (Supplementary Fig. 5), IPSL-CM6A-LR exhibits large-scale anomalies associated with event intensity that are similar to observations (Fig. 6c). Other models also show similar results (Supplementary Figs. 2-3). Most of them simulate coherent changes in wind-stress anomalies and thermocline depth anomalies over the equatorial Pacific, as well as extra-tropical anomalies comparable to observations, during El Niño and La Niña events. Interestingly, IPSL-CM6A-LR shows very little ensemble spread in equatorial Pacific SSTa, while the strength of extra-tropical anomalies and equatorial thermocline responses strongly differ from one simulation to another (Fig 6c).

Impact of decadal variations on future scenarios for ENSO diversity

We next examine ENSO location and intensity in climate change projections, using a set of models that produce variability in ENSO diversity closer to observations during the historical period (namely, IPSL-CM6-LR, UKESM-1-0-LL and CNRM-CM5; Fig. 7). A comparison of future scenarios of ENSO diversity in other models, favouring either EP- and CP-ENSO during historical and pre-industrial periods, is given in Supplementary Fig. 6.

According to IPSL-CM6-LR and UKESM-0-LL, most ensemble members converge to more CP-ENSO over the second half of the 21st century (Fig. 7). This shift to more westward events appears quite early in IPSL-CM6-LR, while it only emerges in the second half of the 21st century in UKESM1-0-LL, as the first half of the 21st century is dominated by decadal

variations (Fig. 7). Such decadal variations remain stronger than potential trends throughout the 21st century in CNRM-CM5 (Fig. 7). By contrast, the last generation of the same model (*i.e.* CNRM-CM6-1), which underestimates decadal variability (Fig. 5), shows a clear shift toward more CP-ENSO in the second half of the 21st century (Supplementary Fig. 6). Future pathways for both El Niño and La Niña locations are strongly dependent on the magnitude of decadal variations, and on the ability of state-of-the-art models to reproduce them. Hence, projections of ENSO diversity show significant discrepancies among models, partly due to models' limitations in accurately representing ENSO diversity, and its variability (as illustrated with MIROC6 and CESM2; Supplementary Fig. 6). Nevertheless, our results overall strongly suggest a shift toward more CP-ENSO as a response to increased radiative forcing over the 21st century (Fig. 7; Supplementary Fig. 6). This corroborates previous hypotheses on the recent increase in the frequency of CP-ENSO[13–16].

While previous studies suggested an intensification of both El Niño and La Niña events over the 21st century[30,31], such trends are hardly distinguishable in models producing realistic ENSO diversity, according to our framework (Fig. 7). In most models, event-intensity and the frequency of extreme events appear, at least, as variable in the 21st century as during the historical period (Fig. 7). However, some models, such as IPSL-CM6-LR (in the second half of the 21st century; Fig. 7, left) and MIROC6 (from the early- to mid-20th century; Supplementary Fig. 6, middle), do show an intensification of ENSO events. In addition, as highlighted in previous studies [30,31], those models show an increase in the frequency of extreme events (Fig. 7; Supplementary Fig 6). Although the reliability of MIROC6 simulations is questionable, considering their generally weaker performances in simulating event-location, their results suggest a potential role of anthropogenic climate change in altering ENSO intensity over the 21st century. Thus, our results highlight that future changes in ENSO characteristics

are not necessarily monotonic, as usually assumed, but may undergo large-amplitude decadal variations, leading to the suppression or enhancement of the impact of anthropogenic climate change on ENSO diversity from one decade to another.

Discussion

To overcome existing limitations in analysing ENSO diversity, this study introduces a new "non-parametric" framework that enables analysis of probabilistic changes in the location and intensity of warm and cold ENSO events. Using multiple century-long observational datasets and state-of-the-art climate models (namely, CMIP5 and CMIP6 ensembles), we first identified robust long-term changes and variability in the likelihood of El Niño and La Niña location and intensity. Although the majority of models favour either EP/Canonical- or CP-ENSO, we found that ENSO diversity is closely linked to significant decadal variations in both observations and climate models. These decadal variations do not only modulate event-intensity, as already highlighted in many studies[17,20,21,45], but also affect event-location, converging toward multiple preferential locations in the central and eastern Pacific.

Despite large underestimations in equatorial zonal wind-stress and thermocline response, we identified robust large-scale patterns associated with long-term changes in ENSO location and intensity using observations and climate models. On the one hand, long-term changes in event-location are associated with zonal perturbation in equatorial wind-stress, which, according to previous studies[22,53,55], may be related to the North Pacific climate variability, and with modulations of the thermocline response. On the other hand, long-term changes in event-intensity are associated with strong equatorial wind-stress and thermocline response, whose variability appears associated with the North and South Pacific climate variability.

The analysis of a realistic set of climate models in terms of ENSO diversity and its variability indicates that magnitude of such decadal variations in the likelihood of ENSO locations and intensity appears even more pronounced than any trend induced by anthropogenic climate change, at least over the first half of the 21st century. Nevertheless, our results strongly suggest a tendency toward more CP-ENSO in response to anthropogenic climate change, which appears more likely over the second half of the 21st century. Similarly, while previous studies suggested an intensification of both El Niño and La Niña events over the 21st century[30,31], such trends are only detected in few models using our framework. In most CMIP5 and CMIP6 models, any potential trends in ENSO intensity, which might be attributed to anthropogenic climate change, appear strongly modulated by decadal variations. Our results thus highlight that future scenarios for ENSO diversity, concerning either event-location or event-intensity, strongly depend on the magnitude of decadal variations, as well as the ability of climate models to reproduce them realistically over the 21st century. Although the nature of such decadal variations is not completely understood[17,19], and could involve non-linear interactions between natural variability and anthropogenic climate change[58], our study provides a new perspective for assessing changes in ENSO behaviour on multiple timescales in a changing climate.

Methods

Observational reference datasets

We use five observational datasets, covering all the different ways to reconstruct long-term variability for SST, as well as different resolutions (Supplementary Table 1). This includes three observational reconstructions based on empirical orthogonal functions/teleconnections (EOF/EOTs), spanning the period 1870-2018: i) the extended reconstructed SST version 5[59] (ERSST.v5); ii) the Centennial in-situ Observation-Based Estimates[60] (COBESST.v2); iii) the

Hadley Centre SST data set[61] (HadSST1). As the use of EOF/EOTs might lead to underestimate ENSO diversity in the 19th and early 20th centuries[24], observational reconstructions are compared to the eight-member ensemble of ocean reanalysis generated using the Simple Ocean Data Assimilation system with sparse observational input version 3[62] (SODA.si3) between 1870 and 2015. Since the use of satellite observations at the end of 20th century is known to result in a cold bias in HadSST1 and COBESST.v2 [63], the optimum interpolation SST version 2[64] (OISST.v2) is used for comparison between 1981 and 2018.

To examine the potential large-scale patterns associated with changes in the ENSO spatio-temporal variability, surface wind-stress was derived from surface zonal and meridional winds for the period 1870-2015, using the NOAA-CIRES-DOE Twentieth Century Reanalysis version 3[65] (NOAA-20CR.v3). The NOAA-20CR.v3 uses SODA.si3 and HadSST1 as boundary forcing, and therefore provides consistent atmospheric circulations for that SST datasets. Because subsurface potential temperature data are not currently available in SODA.si3, we use SODA.v2.2.4, with NOAA-20CR.v2 as boundary forcing, to provide the most consistent estimate of thermocline depth, using the 20°C isotherm depth (Z20) as a proxy.

CMIP5/6 simulations

We use 95 ensemble members of historical simulations from 26 CMIP5 models[40], and 250 members from 28 CMIP6[41] models, together with longer piControl runs (Supplementary Table 1), to evaluate how climate models perform in simulating ENSO diversity. Each individual member of historical simulations allows inferring climate variability from the mid-19th to the early-21st century, due to changes in anthropogenic and natural forcings, while accounting for uncertainties associated with internal variability[66]. Similarly, piControl simulations enable assessing the uncertainties associated with the limited length of reliable historical records. In

addition, to discuss the implications of our results for future scenarios of ENSO diversity, we use the highest emission scenario or forcing level (8.5W.m^{-2}), *i.e.* the Representative Concentration Pathway RCP8.5 in CMIP5 models, and the Shared Socio-economical Pathway 5 that updates the highest forcing level, *i.e.* 8.5W.m^{-2} (SSP5–85) in CMIP6 models. The number of available realisations is substantially lower in future scenarios than historical runs (Supplementary Table 1). Monthly fields of SST, zonal and meridional wind-stress and potential temperature (from which we estimated the thermocline depth from Z20) are used. To ensure consistency with the observational datasets, and to optimise the detection of changing locations and intensity in ENSO, model simulations were all interpolated onto a regular 1.25×1.25° grid in the ocean and the atmosphere.

Examining long-term variability and changes in ENSO location and intensity

To better account for multi-dimensionally varying properties of ENSO, building on the CHI concept[24,25] and recent recommendations[67], we introduce a new framework estimating the location and intensity of El Niño and La Niña events at higher-resolution. The location of El Niño (La Niña) events has been defined as the longitudinal location of the maximum (minimum) of SSTa, greater (lower) than 0°C, within a strip that spans the tropical Pacific from 150°E to 60°W (excluding the warm-pool region), and averaged between 5°S and 5°N over the boreal winter-months (December to February). Meanwhile, the intensity of events is given by the value of the maximum of SSTa at that location and during the same season. SSTa are calculated by removing the mean and trend of each month. Detrending is performed using a locally estimated scatter-plot smoothing. In addition, to harmonize the results over variable grid-resolutions, and reduce the noise in the signal, the location of the maximum and minimum of SSTa has been estimated using a 2° longitudinal smoothing.

Using this new framework, we first examine the likelihood of event location and intensity using the probability density functions (PDF). Temporal changes in the likelihood of event location and intensity are first examined by estimating the PDF over every 20-year segments of each observational datasets, and calculating the most likely values (*i.e*. the mode in statistical terms), as well as multi-dataset agreements of high probability (*i.e.* probability exceeding 0.01 and 0.4 for event location and intensity, respectively). For each 20-year segment, we also quantify the percentage of disagreement in the probability distribution across observational datasets using a Kolmogorov-Smirnov (KS) test at $p = 0.05$. In addition, we examine whether temporal changes in probability distributions of event intensity are associated with changes in the frequency of extreme El Niño (La Niña) events, by quantifying the 20-year average number of events exceeding (lower than) the 90^{th} (10^{th}) percentile across all datasets.

Secondly, we further explore the long-term variability using the 10-year most likely location and intensity of El Niño and La Niña events. Continuous wavelet analyses are used to estimate the maximum power spectrum over the full length of observational and simulated records, while accounting for temporal changes[68]. Using continuous wavelet analysis enables to account for non-stationary significant patches of variability, which might not be significant over the full-length of the records, and would not be identified using Fast Fourier Transform. Significance of variability patches are tested at $p=0.05$, based on 1000 Monte-Carlo simulations of the red noise background spectrum.

Testing robustness in climate models, identifying large-scale patterns and implications for future scenarios

We first examine whether historical and piControl runs, from CMIP5 and CMIP6 models, are able to reproduce a realistic range of locations and intensities for both El Niño and La Niña

events, by comparing the simulated PDF to multiple observational datasets. This visual comparison is combined with two statistical tests: i) test for multimodality, i.e. the presence of multiple peaks on the PDF, based on kernel density estimators and the quantification of excess mass[69]; ii) test for difference in the mean using a two-sided student *t*-test (cf. Supplementary Fig. 1). Statistical significance of these tests is calculated using 1000 permutations.

Secondly, we investigate whether significant decadal variability is detectable in climate models, by comparing the simulated maximum power spectra with observations. We then compare the simulated magnitude of decadal variability to the observed one using the centred ratio of standard deviation ($\mathrm{rSD} = 1 - \frac{sd\left(ENSO_{loc}^{int}[obs]^{10yr}\right)}{sd\left(ENSO_{loc}^{int}[sim]^{10yr}\right)} \times 100$). Statistical significance is then assessed by performing a two-sided Fisher's F-test at p=0.05 between every 100-yr segments through the course of climate simulations and every 100-yr segments in the four longer-term observational SST datasets, from which the rate of success is quantified.

Thirdly, we compare the observed large-scale patterns associated with long-term variability in the location and intensity of El Niño and La Niña events to historical simulations from a set of climate models. This consists in examining the differences in the patterns of pan-Pacific SST, wind-stress and thermocline depth at the Equator (5°S – 5°N), which are computed using linear regression during composite El Niño and La Niña years, separately. Statistical significance of the regression patterns is calculated using 1000 permutations. We particularly focus on the IPSL-CM6A-LR large ensemble model, which displayed closer similarities to observations in terms of ENSO diversity, but more information about the overall model performances are provided in Supplementary Figs. 2–5 .

Finally, using RCP8.5 and SSP5–8.5 scenarios from a selected set of climate models, we examine future trajectories for ENSO diversity (*i.e.* location and intensity), and analyse how results differ depending on the skill of those models for simulating ENSO diversity and its variability.

Data availability

CMIP5 and CMIP6 data are publicly available at https://esgf-index1.ceda.ac.uk. Long-term observational SST datasets, i.e. ERSST.v5, COBESST.v2, HadSST1, OISST.v2, are available at https://climexp.knmi.nl. SODA.si3 and SODA.v2.2.4 are respectively available from https://psl.noaa.gov/data/gridded/data.20thC_ReanV3.html and https://iridl.ldeo.columbia.edu/SOURCES/.CARTON-GIESE/.SODA/.v2p2p4.

Code availability

The code used in this study to produce the data analysed were developed in R programming, and can be provided upon reasonable request to BD.

References

1. McPhaden, M. J., Zebiak, S. E. & Glantz, M. H. ENSO as an Integrating Concept in Earth Science. *Science* **314**, 1740 (2006).
2. Ng, J. Y., Turner, S. W. D. & Galelli, S. Influence of El Niño Southern Oscillation on global hydropower production. *Environmental Research Letters* **12**, 034010 (2017).
3. Iizumi, T. *et al.* Impacts of El Niño Southern Oscillation on the global yields of major crops. *Nature Communications* **5**, 3712 (2014).
4. Goddard, L. & Mason, S. Sensitivity of seasonal climate forecasts to persisted SST anomalies. *Climate Dynamics* **19**, 619–632 (2002).
5. Hermanson, L. *et al.* Different types of drifts in two seasonal forecast systems and their dependence on ENSO. *Climate Dynamics* **51**, 1411–1426 (2018).
6. Dunstone, N. *et al.* Skilful interannual climate prediction from two large initialised model ensembles. *Environmental Research Letters* **15**, 094083 (2020).
7. Capotondi, A. *et al.* Understanding ENSO Diversity. *Bulletin of the American Meteorological Society* **96**, 921–938 (2015).
8. Timmermann, A. *et al.* El Niño–Southern Oscillation complexity. *Nature* **559**, 535–545 (2018).
9. Capotondi, A., Wittenberg, A. T., Kug, J., Takahashi, K. & McPhaden, M. J. ENSO Diversity. in *El Niño Southern Oscillation in a Changing Climate (eds M.J. McPhaden, A. Santoso and W. Cai)* (2020). doi:10.1002/9781119548164.ch4.

10. Cai, W., van Rensch, P., Cowan, T. & Sullivan, A. Asymmetry in ENSO Teleconnection with Regional Rainfall, Its Multidecadal Variability, and Impact. *Journal of Climate* **23**, 4944–4955 (2010).
11. Preethi, B., Sabin, T. P., Adedoyin, J. A. & Ashok, K. Impacts of the ENSO Modoki and other Tropical Indo-Pacific Climate-Drivers on African Rainfall. *Scientific Reports* **5**, 16653 (2015).
12. Sohn, S.-J., Tam, C.-Y. & Kug, J.-S. How does ENSO diversity limit the skill of tropical Pacific precipitation forecasts in dynamical seasonal predictions? *Climate Dynamics* **53**, 5815–5831 (2019).
13. Lee, T. & McPhaden, M. J. Increasing intensity of El Niño in the central-equatorial Pacific. *Geophysical Research Letters* **37**, (2010).
14. Feng, Y., Chen, X. & Tung, K.-K. ENSO diversity and the recent appearance of Central Pacific ENSO. *Climate Dynamics* **54**, 413–433 (2020).
15. Freund, M. B. *et al.* Higher frequency of Central Pacific El Niño events in recent decades relative to past centuries. *Nature Geoscience* **12**, 450–455 (2019).
16. Yeh, S.-W. *et al.* El Niño in a changing climate. *Nature* **461**, 511–514 (2009).
17. Wittenberg, A. T., Rosati, A., Delworth, T. L., Vecchi, G. A. & Zeng, F. ENSO Modulation: Is It Decadally Predictable? *Journal of Climate* **27**, 2667–2681 (2014).
18. Newman, M., Wittenberg, A. T., Cheng, L., Compo, G. P. & Smith, C. A. The Extreme 2015/16 El Niño, in the Context of Historical Climate Variability and Change. *Bulletin of the American Meteorological Society* **99**, S16–S20 (2018).
19. Capotondi, A. & Sardeshmukh, P. D. Is El Niño really changing? *Geophysical Research Letters* **44**, 8548–8556 (2017).
20. Wittenberg, A. T. Are historical records sufficient to constrain ENSO simulations? *Geophysical Research Letters* **36**, (2009).
21. Choi, J., An, S.-I. & Yeh, S.-W. Decadal amplitude modulation of two types of ENSO and its relationship with the mean state. *Climate Dynamics* **38**, 2631–2644 (2012).
22. Newman, M. *et al.* The Pacific Decadal Oscillation, Revisited. *Journal of Climate* **29**, 4399–4427 (2016).
23. Hu, S. & Fedorov, A. v. Cross-equatorial winds control El Niño diversity and change. *Nature Climate Change* **8**, 798–802 (2018).
24. Giese, B. S. & Ray, S. El Niño variability in simple ocean data assimilation (SODA), 1871–2008. *Journal of Geophysical Research: Oceans* **116**, (2011).
25. Ray, S. & Giese, B. S. Historical changes in El Niño and La Niña characteristics in an ocean reanalysis. *Journal of Geophysical Research: Oceans* **117**, (2012).
26. Capotondi, A., Wittenberg, A. & Masina, S. Spatial and temporal structure of Tropical Pacific interannual variability in 20th century coupled simulations. *Ocean Modelling* **15**, 274–298 (2006).
27. Bellenger, H., Guilyardi, E., Leloup, J., Lengaigne, M. & Vialard, J. ENSO representation in climate models: from CMIP3 to CMIP5. *Climate Dynamics* **42**, 1999–2018 (2014).
28. Dieppois, B., Rouault, M. & New, M. The impact of ENSO on Southern African rainfall in CMIP5 ocean atmosphere coupled climate models. *Climate Dynamics* **45**, 2425–2442 (2015).
29. Ham, Y.-G. & Kug, J.-S. How well do current climate models simulate two types of El Nino? *Climate Dynamics* **39**, 383–398 (2012).
30. Cai, W. *et al.* Increased frequency of extreme La Niña events under greenhouse warming. *Nature Climate Change* **5**, 132–137 (2015).
31. Cai, W. *et al.* Increasing frequency of extreme El Niño events due to greenhouse warming. *Nature Climate Change* **4**, 111–116 (2014).
32. Grothe, P. R. *et al.* Enhanced El Niño–Southern Oscillation Variability in Recent Decades. *Geophysical Research Letters* **47**, e2019GL083906 (2020).
33. Rasmusson, E. M. & Carpenter, T. H. Variations in Tropical Sea Surface Temperature and Surface Wind Fields Associated with the Southern Oscillation/El Niño. *Monthly Weather Review* **110**, 354–384 (1982).
34. Kao, H.-Y. & Yu, J.-Y. Contrasting Eastern-Pacific and Central-Pacific Types of ENSO. *Journal of Climate* **22**, 615–632 (2009).
35. Takahashi, K., Montecinos, A., Goubanova, K. & Dewitte, B. ENSO regimes: Reinterpreting the canonical and Modoki El Niño. *Geophysical Research Letters* **38**, (2011).
36. Trenberth, K. E. & Stepaniak, D. P. Indices of El Niño Evolution. *Journal of Climate* **14**, 1697–1701 (2001).
37. Ashok, K., Behera, S. K., Rao, S. A., Weng, H. & Yamagata, T. El Niño Modoki and its possible teleconnection. *Journal of Geophysical Research: Oceans* **112**, (2007).
38. Dommenget, D., Bayr, T. & Frauen, C. Analysis of the non-linearity in the pattern and time evolution of El Niño southern oscillation. *Climate Dynamics* **40**, 2825–2847 (2013).
39. Kug, J.-S. & Ham, Y.-G. Are there two types of La Nina? *Geophysical Research Letters* **38**, (2011).

40. Taylor, K. E., Stouffer, R. J. & Meehl, G. A. An Overview of CMIP5 and the Experiment Design. *Bulletin of the American Meteorological Society* **93**, 485–498 (2012).
41. Eyring, V. *et al.* Overview of the Coupled Model Intercomparison Project Phase 6 (CMIP6) experimental design and organization. *Geosci. Model Dev.* **9**, 1937–1958 (2016).
42. Hu, Z.-Z., Huang, B., Zhu, J., Kumar, A. & McPhaden, M. J. On the variety of coastal El Niño events. *Climate Dynamics* **52**, 7537–7552 (2019).
43. Rodrigues, R. R., Subramanian, A., Zanna, L. & Berner, J. ENSO Bimodality and Extremes. *Geophysical Research Letters* **46**, 4883–4893 (2019).
44. Johnson, N. C. How Many ENSO Flavors Can We Distinguish? *Journal of Climate* **26**, 4816–4827 (2013).
45. Sun, F. & Yu, J.-Y. A 10–15-Yr Modulation Cycle of ENSO Intensity. *Journal of Climate* **22**, 1718–1735 (2009).
46. Deser, C. *et al.* ENSO and Pacific Decadal Variability in the Community Climate System Model Version 4. *Journal of Climate* **25**, 2622–2651 (2012).
47. Capotondi, A., Deser, C., Phillips, A. S., Okumura, Y. & Larson, S. M. ENSO and Pacific Decadal Variability in the Community Earth System Model Version 2. *Journal of Advances in Modeling Earth Systems* **12**, e2019MS002022 (2020).
48. Mann, M. E., Steinman, B. A. & Miller, S. K. Absence of internal multidecadal and interdecadal oscillations in climate model simulations. *Nature Communications* **11**, 49 (2020).
49. Ault, T. R., Deser, C., Newman, M. & Emile-Geay, J. Characterizing decadal to centennial variability in the equatorial Pacific during the last millennium. *Geophysical Research Letters* **40**, 3450–3456 (2013).
50. Power, S., Delage, F., Wang, G., Smith, I. & Kociuba, G. Apparent limitations in the ability of CMIP5 climate models to simulate recent multi-decadal change in surface temperature: implications for global temperature projections. *Climate Dynamics* **49**, 53–69 (2017).
51. Capotondi, A. & Sardeshmukh, P. D. Optimal precursors of different types of ENSO events. *Geophysical Research Letters* **42**, 9952–9960 (2015).
52. Fang, X.-H. & Mu, M. A Three-Region Conceptual Model for Central Pacific El Niño Including Zonal Advective Feedback. *Journal of Climate* **31**, 4965–4979 (2018).
53. McPhaden, M. J., Lee, T. & McClurg, D. El Niño and its relationship to changing background conditions in the tropical Pacific Ocean. *Geophysical Research Letters* **38**, (2011).
54. Taschetto, A. S., Rodrigues, R. R., Meehl, G. A., McGregor, S. & England, M. H. How sensitive are the Pacific–tropical North Atlantic teleconnections to the position and intensity of El Niño-related warming? *Climate Dynamics* **46**, 1841–1860 (2016).
55. Larson, S. & Kirtman, B. The Pacific Meridional Mode as a trigger for ENSO in a high-resolution coupled model. *Geophysical Research Letters* **40**, 3189–3194 (2013).
56. di Lorenzo, E. *et al.* ENSO and meridional modes: A null hypothesis for Pacific climate variability. *Geophysical Research Letters* **42**, 9440–9448 (2015).
57. Liguori, G. & di Lorenzo, E. Separating the North and South Pacific Meridional Modes Contributions to ENSO and Tropical Decadal Variability. *Geophysical Research Letters* **46**, 906–915 (2019).
58. Cai, W. *et al.* Butterfly effect and a self-modulating El Niño response to global warming. *Nature* **585**, 68–73 (2020).
59. Huang, B. *et al.* Extended Reconstructed Sea Surface Temperature, Version 5 (ERSSTv5): Upgrades, Validations, and Intercomparisons. *Journal of Climate* **30**, 8179–8205 (2017).
60. Hirahara, S., Ishii, M. & Fukuda, Y. Centennial-Scale Sea Surface Temperature Analysis and Its Uncertainty. *Journal of Climate* **27**, 57–75 (2014).
61. Rayner, N. A. *et al.* Global analyses of sea surface temperature, sea ice, and night marine air temperature since the late nineteenth century. *Journal of Geophysical Research: Atmospheres* **108**, (2003).
62. Giese, B. S., Seidel, H. F., Compo, G. P. & Sardeshmukh, P. D. An ensemble of ocean reanalyses for 1815–2013 with sparse observational input. *Journal of Geophysical Research: Oceans* **121**, 6891–6910 (2016).
63. Reynolds, R. W., Rayner, N. A., Smith, T. M., Stokes, D. C. & Wang, W. An Improved In Situ and Satellite SST Analysis for Climate. *Journal of Climate* **15**, 1609–625 (2002).
64. Banzon, V., Smith, T. M., Steele, M., Huang, B. & Zhang, H.-M. Improved Estimation of Proxy Sea Surface Temperature in the Arctic. *Journal of Atmospheric and Oceanic Technology* **37**, 341–349 (2020).
65. Slivinski, L. C. *et al.* Towards a more reliable historical reanalysis: Improvements for version 3 of the Twentieth Century Reanalysis system. *Quarterly Journal of the Royal Meteorological Society* **145**, 2876–2908 (2019).

66. Deser, C., Phillips, A., Bourdette, V. & Teng, H. Uncertainty in climate change projections: the role of internal variability. *Climate Dynamics* **38**, 527–546 (2012).
67. Planton, Y. Y. *et al.* Evaluating Climate Models with the CLIVAR 2020 ENSO Metrics Package. *Bulletin of the American Meteorological Society* **102**, E193–E217 (2021).
68. Torrence, C. & Compo, G. P. A Practical Guide to Wavelet Analysis. *Bulletin of the American Meteorological Society* **79**, 61–78 (1998).
69. Ameijeiras-Alonso, J., Crujeiras, R. M. & Rodríguez-Casal, A. Mode testing, critical bandwidth and excess mass. *TEST* **28**, 900–919 (2019).

Acknowledgements

This work is part of the I-SITE Bourgogne Franche-Comté Junior Fellowship IMVULA (AAP2-JF-06). AC was supported by the NOAA Climate Program Office's Climate Variability and Predictability (CVP) and Modelling, Analysis, Predictions and Projections (MAPP) programs. The authors would like to thank Noel Keenlyside and Lander Crespo (Geophysical Institute, University of Bergen) for their helpful discussions.

Captions

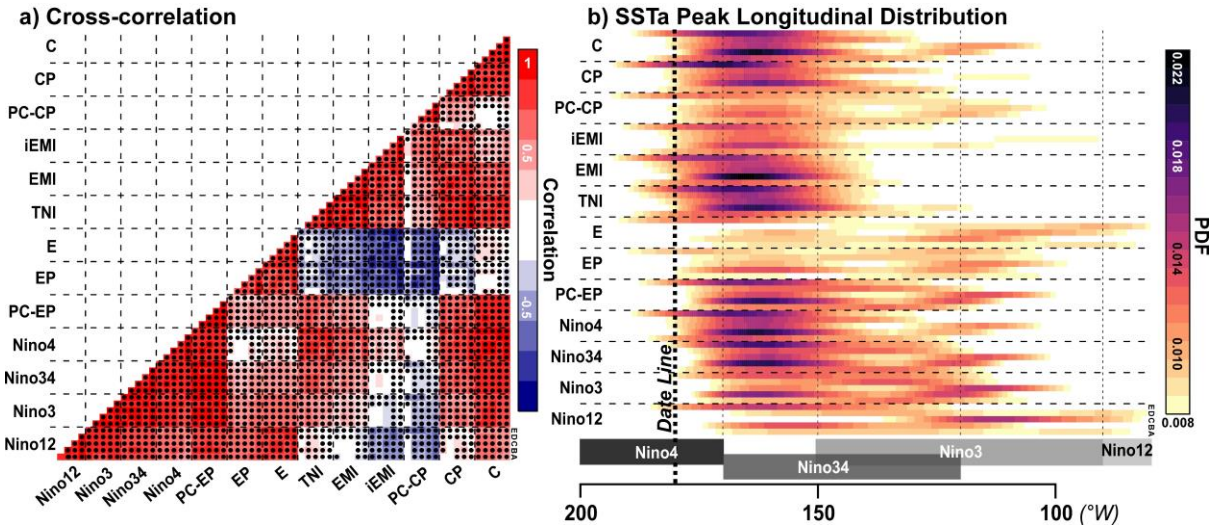

Fig 1. | Relationships between ENSO indices, and their ability to disentangle CP and EP. **(a)** Pearson's correlations between 13 ENSO indices (Niño boxes[33]; PC-based EP- and CP-ENSO; TNI[36]; EMI and iEMI[37]; EP and CP[34]; E and C[35]. Black dots indicate significant correlations at p=0.05, using 1000 phase-randomizations to account for serial correlations. **(b)** Probability Density Function (PDF) of the locations of SSTa peaks over the equatorial Pacific (5°S–5°N; -210–-60°W), when each ENSO index exceeds ±0.5°C standard deviation. For each index, each row/column corresponds to a different observational, reanalysis or satellite-derived dataset (A-E: ERSST.v5, COBESST.v2, HadSST1, SODA.si3, OISST.v2). Correlations are calculated over their respective common periods (1870-2017 when using observations only, 1870-2015 when using SODA.si3, or 1981-2017 when using OISST.v2). Locations of Niño boxes, as well as of the date line, are indicative.

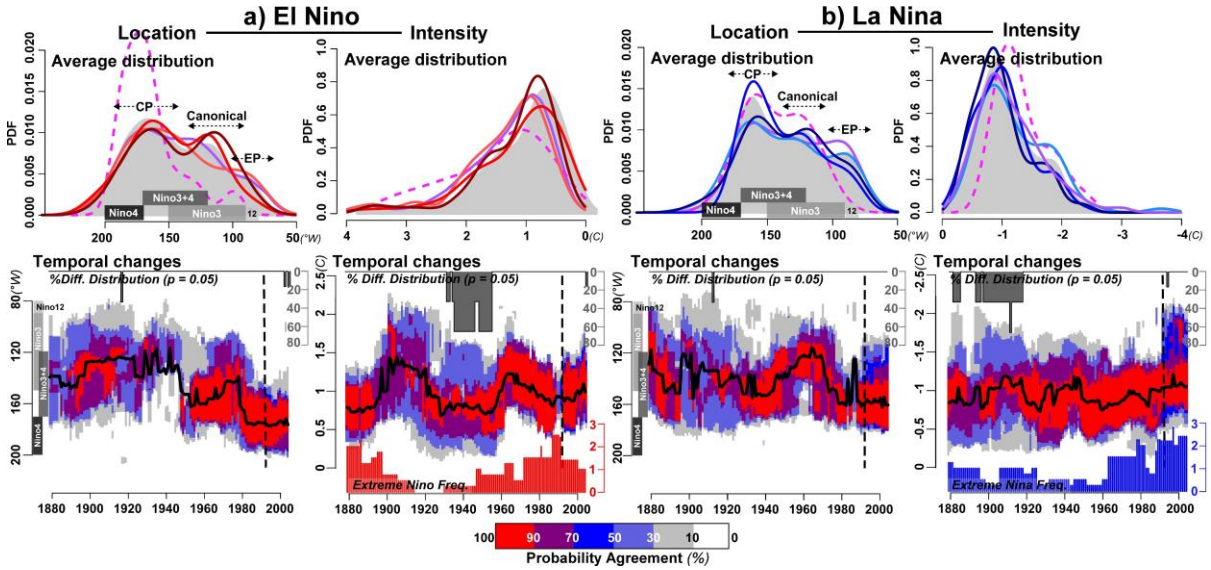

Fig 2. | Observed likelihood of ENSO's location and intensity: average distribution and temporal changes. (a) top panels, average probability density function (PDF) of El Niño location (left) and intensity (right). Bottom panels, 20-year running the most likely location and intensity of El Niño (black bold lines), the percentage of agreement of high-probability (*i.e.* PDF exceeding 0.01 and 0.45; colour shades), and average number of extreme Niño events (*i.e.* intensity exceeding the 90th percentile; red histogram) across all observational datasets. **(b)** same as **(a)** but for La Niña, and extreme La Niña events (*i.e.* intensity lower than the 10th percentile; blue histogram). On top panels, dark grey shading from the top axis indicates the average PDF over all five reference SST datasets, and each individual dataset is displayed in coloured lines (El Niño/La Niña: ERSST.v5 [1850-2017; coral/light blue], COBESST.v2 [1850-2017; dark red/dark blue], HadSST1 [1850-2017; red/blue], SODA.si3 [1850-2015; purple solid lines], OISST.v2 [1981-2017; magenta dashed lines]). On bottom panels, grey shading indicates the percentage of observational datasets showing significantly equal distribution at p=0.05 according to a Kolmogorov-Smirnov test. Locations of Nino boxes, as well as of the date line, are indicative. Dashed lines delineate the period for which OISST.v2 is used (1991-2007, which covers 20-yr periods between 1981-2001 and 1997-21017).

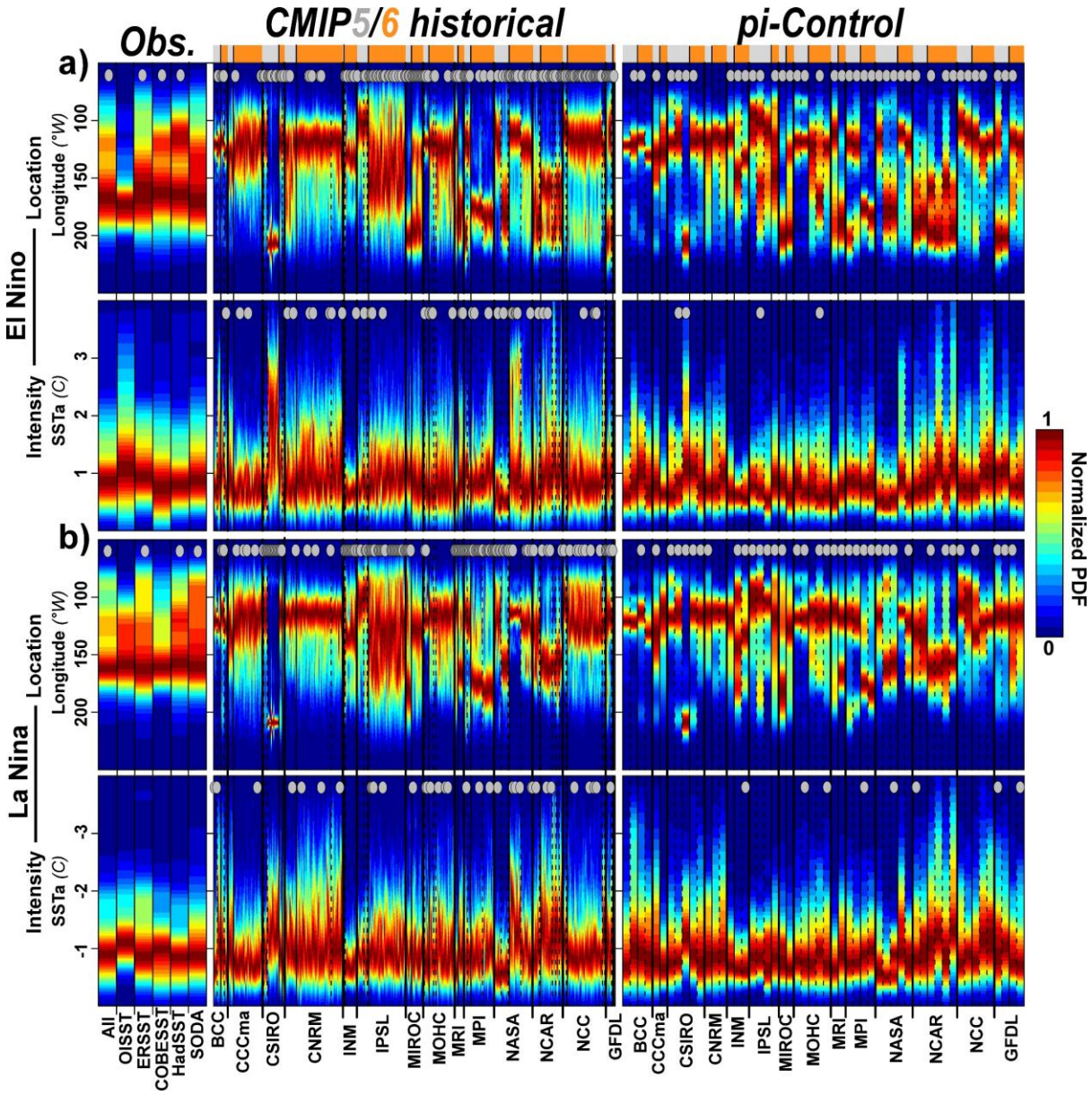

Fig 3. | Likelihood of ENSO's location and intensity in CMIP5 and CMIP6 models. (a) top panels, normalized PDF of El Niño location (top) and intensity (bottom) in all reference datasets (left), as compared to 95/250 CMIP5/6 historical runs (middle), as well as in 26/28 CMIP5/6 piControl runs (right). **(b)** same as **(a)** but for La Niña. On top of each panel and column, grey dots indicate significant multimodality at p=0.05 according to the ACR test[69], based on 1000 bootstrap resamples. The normalized PDF is estimated using the full length of each time series, ranging from 37 years in OISST.v2 to 1200 years in some piControl simulations. Bold (thin) solid lines separate simulations from different institutions (generations, i.e.: CMIP5 [grey] and CMIP6 [orange]), while dashed lines separate simulations from different models.

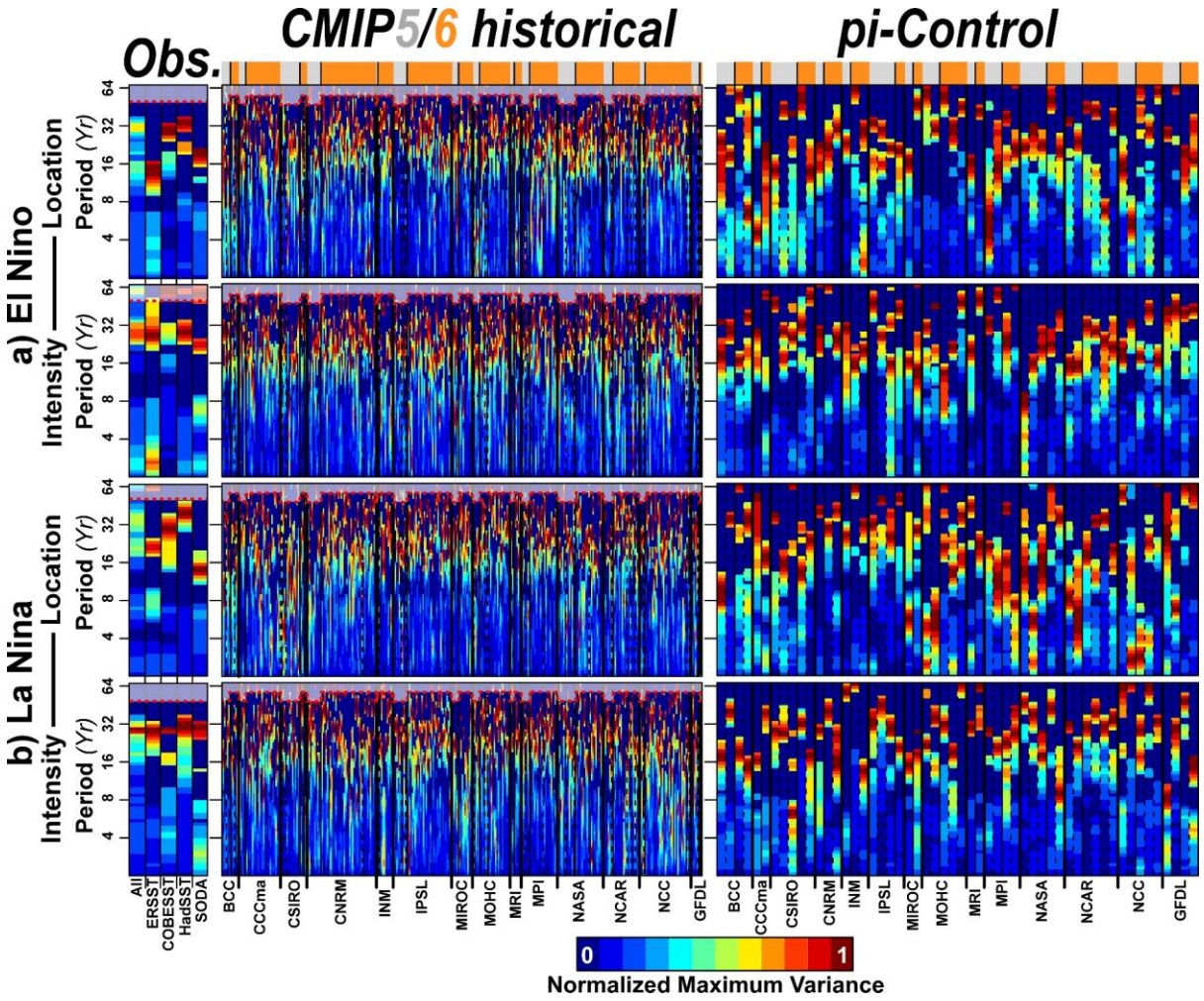

Fig 4. | Variability in ENSO's, observed and simulated, most likely location and intensity. **(a)** Maximum power spectrums of the running 10-year El Niño most likely location and intensity (i.e. the mode), as determined using continuous wavelet analysis, and using four long-term observational reference datasets (left: ERSST.v5, COBESST.v2, HadSST1, SODA.si3), 95/250 CMIP5/6 historical runs (middle), as well as 26/28 CMIP5/6 piControl runs (right). **(b)** same as **(a)** but for La Niña. Significance of variability patches are tested at p=0.05 based on 1000 Monte-Carlo simulations of the red noise background spectrum. Dashed red lines and grey shading indicate the area where variability can be underestimated because of edge effects, wraparound effects and zero-padding. As the continuous wavelet analysis allows to account for temporal changes the maximum power spectrums are estimated using the full length of each time series. The maximum power spectrums are weighted by the significance, and only significant variability is shown.

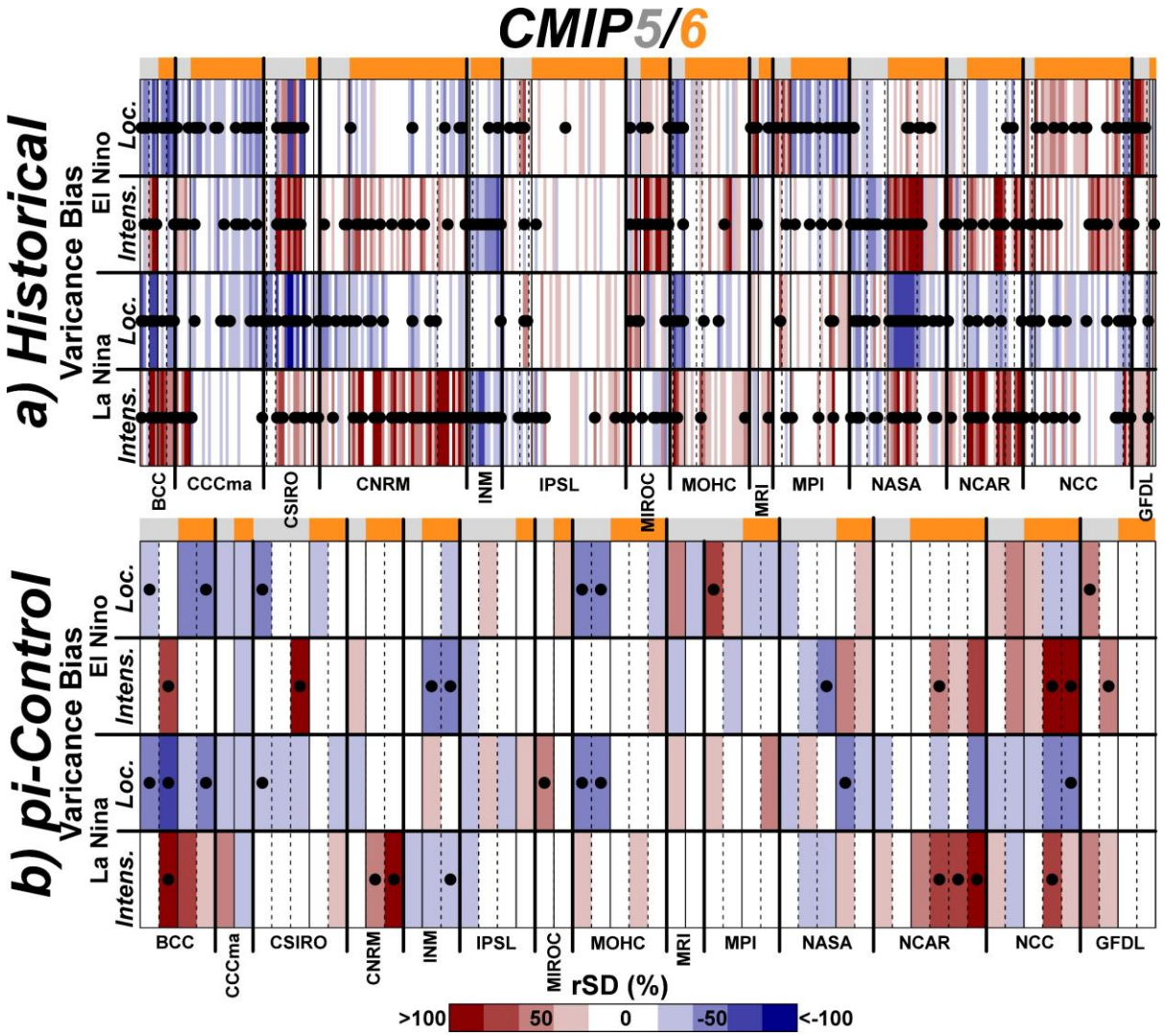

Fig 5. | CMIP5/6 bias in decadal variability of ENSO's most likely location and intensity. **(a)** Average ratio of standard deviation (rSD) between historical runs and observed decadal variance (>10 year) in the running 10-year most likely location and intensity of El Niño and La Niña events. **(b)** same as **(a)** but using pi-Control runs. Statistical significance is assessed by performing a two-sided Fisher's F-test at p=0.05 between every 100-yr segments through the course of climate simulations and every 100-yr segments in the four longer-term observational SST datasets (*i.e.* $27{,}740 \leq n \leq 209{,}000$ replicates), to quantify a rate of success (i.e. the number of times observations and simulations showed equal variance). Black dots highlight simulations for which the rate of success is lower than 10%, showing significantly different variance at p=0.1.

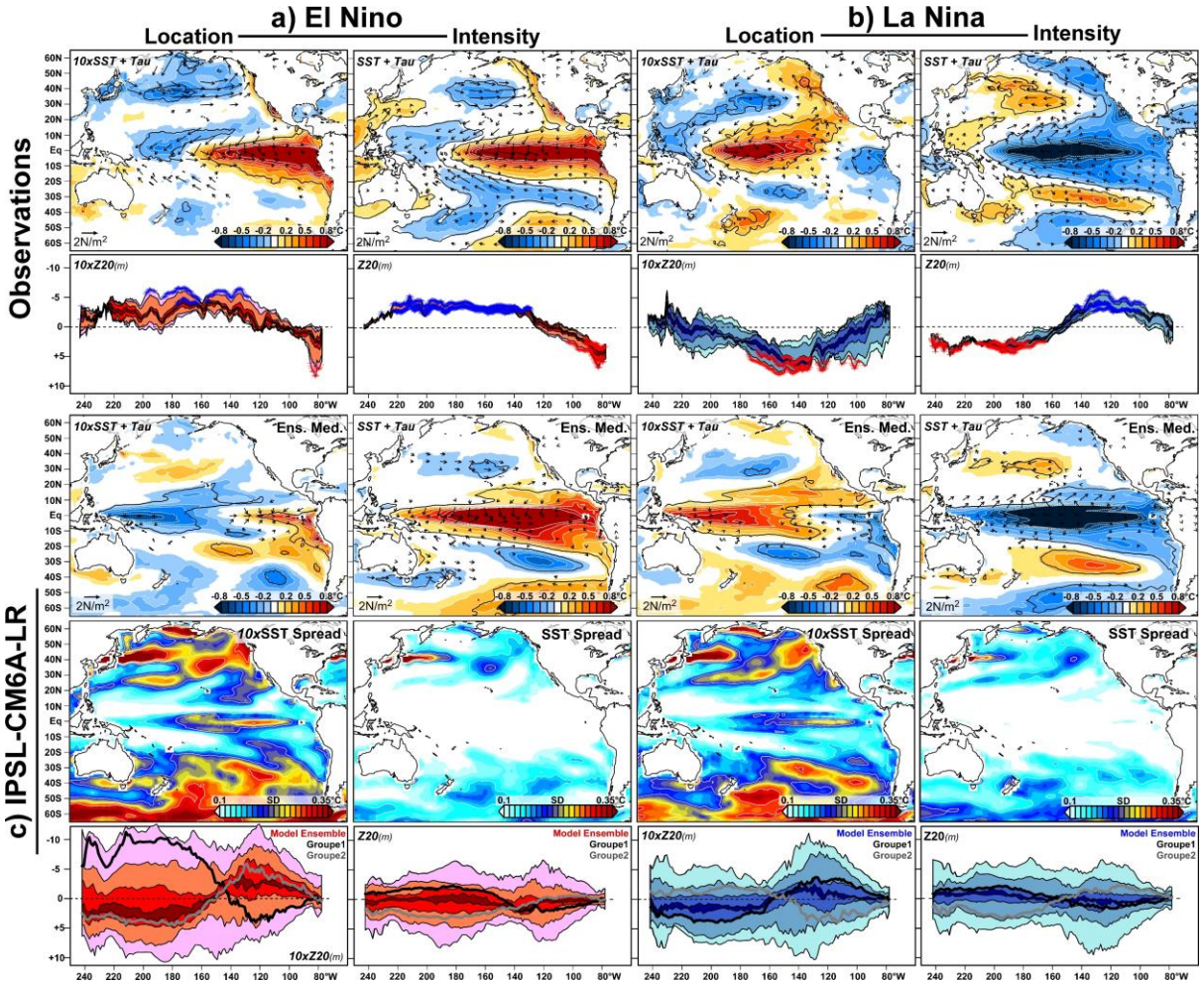

Fig 6. | Large-scale patterns driving long-term variability in ENSO location and intensity. **(a)** Observed regressed SST (blue to red shades), wind-stress (vectors) and Z20 anomalies (lines) associated with changes in El Niño location (right) and intensity (left) and using multiple observational data sets (SST: ERSST.v5, COBESST.v2, HadSST1 and SODA.si3; wind-stress: NOAA-20CR.v3; Z20: SODA.v2.2.4). **(b)** Same as **(a)** but for La Niña events. **(c)** same as **(a-b)** but using the IPSL-CM6A-LR large ensemble (32 members). While SST and wind-stress anomalies are displayed at the pan-Pacific scale based on the median changes in observations, simulated regressed anomalies are assessed through the ensemble median (top) and ensemble spread (standard deviation [SD]; middle]). Z20 anomalies are estimated through the median changes between 5°S and 5°N (bottom). Red and Blue shades on the Z20 anomalies indicate the spread between the four SST observational data sets and within the IPSL-CM6A-LR large ensemble (light to dark: maximum/minimum, 10/90th, 30/70th and 45/55th percentiles), for El Niño and La Niña, respectively. Group 1 (black lines) and Group 2 (grey lines) illustrate how two opposed types of equatorial Z20 anomalies influence the ensemble spread. Statistical significance is assessed at p=0.05 using 1000 permutations, and displayed as black contour for SSTa, and blue/red crosses for Z20 anomalies. Only significant wind-stress anomalies at p=0.05 are displayed.

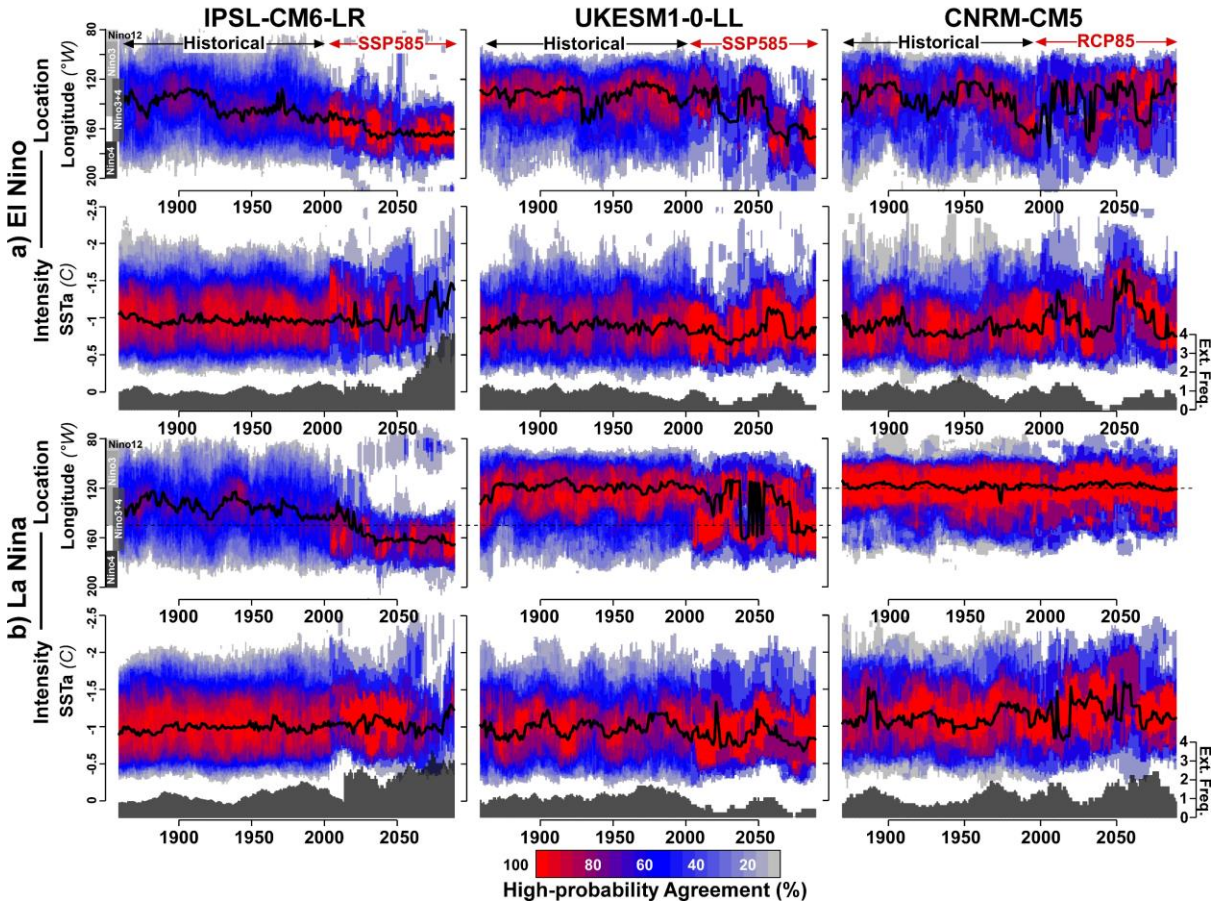

Fig 7. | Future scenarios for ENSO diversity in the most realistic models. (a) 20-year most likely location (top) and intensity (bottom) of El Niño events (black bold lines), as well as the percentage of agreement of high-probability (PDF exceeding 0.01 and 0.45; colour shades) in the IPSL-CM6-LR (left), UKESM1-0-LL (middle) and CNRM-CM5 (right) ensembles. **(b)** same as **(a)** but for La Niña events. Grey histograms on the bottom axis of the intensity panels indicate the average number of extreme events (as defined in Fig. 2) within the model ensemble. SSTa are estimated by removing the 1850–2014 monthly climatology and trend, to allow comparison with observations. The same baseline period was used to estimate the 90th and 10th percentiles.